Johann Radon Institute for
Computational and Applied Mathematics
Austrian Academy of Sciences (ÖAW)

Reconstruction of complex cracks by far field measurements

P. Krutitskii, J. Liu, M. Sini

RICAM-Report 2008-15

Reconstruction of complex cracks by far field measurements

P. Krutitskii* J.J. Liu† M. Sini‡

January 30, 2008

Abstract

In this paper, we deal with the acoustic inverse scattering problem for reconstructing complex cracks from the far field map. The scattering problem models the diffraction of waves by thin two-sided cylindrical screens. A complex crack is characterized by its shape, the type of boundary conditions and the boundary coefficients (surface impedance). We give explicit formulas which can be used to reconstruct the shape of the crack, distinguish its type of boundary conditions, its two faces and reconstruct the possible material coefficients on it by using the far-field map. To test the validity of these formulas, we present some numerical implementations, which show the efficiency of the proposed method for suitably distributed surface impedance. The difficulties for numerically recovering the properties of the crack in the concave side as well as near the tips are presented and some explanations are given.

Key words. Inverse scattering, cracks, far-field, numerics.
AMS subject classifications. 35P25, 35R30, 78A45.

1 Statement of the problem

To describe the diffraction of acoustic waves by thin two-side cylindrical screens, the scattering problems are governed by the Helmholtz equation by a crack Γ in $\mathbb{R}^2$. Let Γ be a two dimensional open curve of class C^3 with a parameterization representation $\Gamma = \{x := x(s), s \in [a,b]\}$ where $x : [a,b] \to \mathbb{R}^2$ is locally of class C^3 . We set $P = x(a)$ and $Q = x(b)$ to be the two tips of Γ, and fix the orientation of Γ as follows. Traveling on Γ from P to Q, we associate to the right side the sign $+$, i.e. Γ^+, and to the left side the sign $-$, i.e. Γ^- and we set ν to be the unit normal on Γ oriented towards Γ^+. The different boundary conditions specified on Γ represent the acoustic properties of the crack. For given incident waves $u^i(x) = e^{i\kappa d\cdot x}$, we consider the following scattering problems for total waves $u(x) = u^i(x) + u^s(x)$:

$$(1.1) \qquad (\text{ Dirichlet }) \begin{cases} (\Delta + \kappa^2)u = 0, & \text{in } \mathbb{R}^2 \setminus \overline{\Gamma}, \\ u = 0 \quad \text{on } \Gamma^{\pm}, \\ u = u^s + e^{i\kappa d\cdot x}, \\ \lim_{r\to\infty} \sqrt{r}(\frac{\partial u^s}{\partial r} - i\kappa u^s) = 0, \end{cases}$$

*KIAM, Miussqaya Sq.4, Moscow, 125047, Russia. email: krutitsk@math.phys.msu.su
†Department of Mathematics, Southeast University, Nanjing, 210096, email: jjliu@seu.edu.cn, P.R.China.
‡RICAM, Austrian Academy of Science, Linz, A-4040, Austria. email: mourad.sini@oeaw.ac.at

$$(1.2) \qquad (\text{ Mixed }) \begin{cases} (\Delta+\kappa^2)u=0, & \text{in } \mathbb{R}^2\setminus\overline{\Gamma}, \\ u=0 \quad \text{on } \Gamma^+, \\ \frac{\partial u^s}{\partial \nu}-i\kappa\sigma_- u^s=0, & \text{on } \Gamma^-, \\ u=u^s+e^{i\kappa d\cdot x}, \\ \lim_{r\to\infty}\sqrt{r}(\frac{\partial u^s}{\partial r}-i\kappa u^s)=0, \end{cases}$$

$$(1.3) \qquad (\text{ Robin }) \begin{cases} (\Delta+\kappa^2)u=0, & \text{in } \mathbb{R}^2\setminus\overline{\Gamma}, \\ \frac{\partial u}{\partial \nu}\pm i\kappa\sigma_\pm u=0, & \text{on } \Gamma^\pm, \\ u=u^s+e^{i\kappa d\cdot x}, \\ \lim_{r\to\infty}\sqrt{r}(\frac{\partial u^s}{\partial r}-i\kappa u^s)=0, \end{cases}$$

where $u^s(x)$ is the scattered wave outside of Γ, while $\kappa>0$ is the wave number and d is the direction of incidence of plane wave $u^i(x)$. We assume that $\sigma^\pm$ are complex valued Holder continuous functions of order $\beta\in(0,1]$, $\sigma_\pm=\sigma_\pm^r+i\sigma_\pm^i$, and their real parts have positive uniform lower bounds.

The problems (1.1), (1.2) and (1.3) are well posed, see [9], [10], [11], [13], and [2] for more details. These models describe the scattering problems of the cracks with different acoustic properties. Using the asymptotic behavior of the fundamental solution , as in [3], we can show that the scattered wave has the asymptotic behavior:

$$(1.4) \qquad u^s(x,d) \quad = \quad \frac{e^{i\kappa r}}{\sqrt{r}}u^\infty(\hat{x},d)+O(r^{-3/2}), \quad r:=|x|\to\infty,$$

where the function $u^\infty(\cdot,d)$ defined on the unit circle S^1 is called the far-field of the scattered wave u^s corresponding to incident direction d. We introduce a constant $\gamma_2:=\frac{e^{i\pi/4}}{\sqrt{8\pi\kappa}}$ and $\Phi(x,y):=\frac{i}{4}H_0^{(1)}(\kappa|x-y|), \quad x\neq y, x,y\in\mathbb{R}^2$, the fundamental solution to the Helmholtz equation in $\mathbb{R}^2$, where $H_0^{(1)}$ is the Hankel function of the first kind of order zero. In this paper, we will consider the following:

Complex crack reconstruction problem. *Given $u^\infty(\cdot,\cdot)$ on $S^1\times S^1$ for the scattering problems (1.1) or (1.2) or (1.3), reconstruct the shape of the crack Γ, distinguish the two faces and reconstruct the eventual surface impedances $\sigma_\pm(x)$.*

REMARK 1.1 *We do not know a priori to which problem is associated the data $u^\infty(\hat{x},d)$ on $(\hat{x},d)\in S^1\times S^1$.*

The inverse problems for cracks detection have been studied by many authors. We refer to [1] for some results concerning, in particular, detection of piecewise linear cracks from one or few exterior measurements. We are interested by detection of cracks of general shapes but using many measurements. Precisely, we use the far field map and our aim is to reconstruct the whole crack. There were several works devoted to the detection of cracks from many measurements. Among others, we shall cite [7], [6] and [2], and the references there, where the authors gave reconstruction methods to detect the shape of the cracks. In this paper, we shall be concerned by reconstructing complex cracks by giving the shapes, the type of boundary conditions, distinguishing the two faces and computing the pointwise values of the complex valued surface impedances distributed along them. Precisely, we provide direct formulas which link the far field map to the unknowns. We show that these formulas contain the information on the cracks throuth an asymptotic expansion

with respect to the point sources used. Hence, we should be careful to what extent these indicators can approximate the crack properties such as its shape, the acoustic properties and the possible surface impedance. Our numerical realizations presented in the last section show that the property of the crack in the convex side can be reconstructed well, but the reconstruction in the concave side of the crack is quite limited. This phenomenon can be explained physically by the multiple reflections of the waves within the cavity, which lead to a relatively less information about the concave side in the far field pattern. In addition appropriate types of variations of the surface impedance can improve the reconstruction in the concave parts but also can destroy the one near the convex parts. This shows how difficult it is to reconstruct numerically the shape of the crack without knowing its properties or some *a-priori* informations. We wish also to point out that our formulas are valid on the points of the crack away from the tips. We believe that the indicator functions near the tips should be more singular. But such an assersion needs to be justified.

The plan of the paper is as follows. In section 2, we present the theoretical results related to the asymptotic formulas by adding some comments on how one can use them. In section 3, we give the justifications of these results and in section 4, we present extensive numerical results followed by some detailed explanations.

2 Presentation of the results

It is well known, see [3], that the scattered field associated with the Herglotz incident field $v_g^i := v_g$ defined by $v_g(x) := \int_{S^1} e^{i\kappa x\cdot d} g(d)\ ds(d)$, $x \in \mathbb{R}^2$ with $g \in L^2(S^1)$ is given by $v_g^s(x) := \int_{S^1} u^s(x,d) g(d)\ ds(d)$, $x \in \mathbb{R}^2 \setminus \Gamma$, and its far field is $v_g^\infty(\hat{x}) := \int_{S^1} u^\infty(\hat{x},d) g(d)\ ds(d)$, $\hat{x} \in S^1$.

We will need the following identity, see [3],

$$u^\infty(\hat{x},d) = -\gamma_2 \int_{\partial D} \left\{ \frac{\partial u^s(y,d)}{\partial \nu} e^{-i\kappa \hat{x}\cdot y} - \frac{\partial e^{-i\kappa \hat{x}\cdot y}}{\partial \nu} u^s(y,d) \right\} ds(y) \tag{2.1}$$

where ∂D is a closed curve containing a part of Γ and avoiding the tips (P,Q). In addition, we assume that the bounded domain surrounded by ∂D, i.e D, is such that $\Gamma \subset \overline{D}$. In particular D contains the tips (P,Q).

Assume that $\Gamma \subset\subset \Omega$ for some known Ω with smooth boundary. For $a \in \Omega \setminus \overline{\Gamma}$, denote by $\{z_p\} \subset \Omega \setminus \overline{D}$ a sequence tending to a. For any z_p, set D_a^p to be a C^2- regular domain such that $\overline{\Gamma} \subset D_a^p$ with $z_q \in \Omega \setminus \overline{D_a^p}$ for every $q = 1, 2, \cdots, p$ and that the Dirichlet interior problem on D_a^p for the Helmholtz equation is uniquely solvable. In this case, the Herglotz wave operator $\mathbb{H}$ defined from $L^2(S^1)$ to $L^2(\partial D_a^p)$ by

$$\mathbb{H}[g](x) := v_g(x) = \int_{S^1} e^{i\kappa x\cdot d} g(d)\ ds(d) \tag{2.2}$$

is injective, compact with dense range, see [3]. Now we consider the sequence of point sources $\Phi(\cdot, z_p)$. For every p fixed, we construct two density sequences $\{g_n^p\}$ and $\{f_m^{j,p}\}$ in $L^2(S^1)$ by the Tikhonov regularization such that

$$||v_{g_n^p} - \Phi(\cdot, z_p)||_{L^2(\partial D_a^p)} \to 0, \quad n \to \infty \tag{2.3}$$

$$||v_{f_m^{j,p}} - \frac{\partial}{\partial x_j}\Phi(\cdot, z_p)||_{L^2(\partial D_a^p)} \to 0, \quad m \to \infty. \tag{2.4}$$

We choose ∂D to contain a part of Γ surrounding the fixed point a, such that $\{z_p\} \subset \Omega \setminus \overline{D}$ (for p large enough) and $\overline{D} \subset D_a^p$. Since both $v_{g_n^p}$ and $\Phi(\cdot, z_p)$ satisfy the same Helmholtz equation in D_a^p, (2.3) implies that

$$||v_{g_n^p} - \Phi(\cdot, z_p)||_{H^{\frac{1}{2}}(\partial D)} \to 0, \quad n \to \infty \tag{2.5}$$

and

$$||\frac{\partial}{\partial \nu} v_{g_n^p} - \frac{\partial}{\partial \nu}\Phi(\cdot, z_p)||_{H^{-\frac{1}{2}}(\partial D)} \to 0, \quad n \to \infty \tag{2.6}$$

Similarly, it follows from (2.4) that

$$||v_{f_m^{j,p}} - \frac{\partial}{\partial x_j}\Phi(\cdot, z_p)||_{H^{\frac{1}{2}}(\partial D)} \to 0, \quad m \to \infty \tag{2.7}$$

and

$$||\frac{\partial}{\partial \nu} v_{f_m^{j,p}} - \frac{\partial}{\partial \nu}(\frac{\partial}{\partial x_j}\Phi(\cdot, z_p))||_{H^{-\frac{1}{2}}(\partial D)} \to 0, \quad m \to \infty \tag{2.8}$$

Multiplying (2.1) by $f_m^{j,p}(d) g_n^p(\hat{x})$ and integrating over $S^1 \times S^1$, we have

$$\begin{aligned}
& -\int_{S^1}\int_{S^1} u^\infty(-\hat{x}, d) f_m^{j,p}(d) g_n^p(\hat{x})\, ds(\hat{x}) ds(d) \\
= \; & \gamma_2 \int_{\partial D} \left\{ \int_{S^1} \frac{\partial u^s(y,d)}{\partial \nu} f_m^{j,p}(d)\, ds(d) \cdot \int_{S^1} e^{i\kappa \hat{x}\cdot y} g_n^p(\hat{x})\, ds(\hat{x}) - \right. \\
& \left. \int_{S^1} \frac{\partial e^{i\kappa\hat{x}\cdot y}}{\partial \nu} g_n^p(\hat{x})\, ds(\hat{x}) \cdot \int_{S^1} u^s(y,d) f_m^{j,p}(d)\, ds(d) \right\} ds(y) \\
= \; & \gamma_2 \int_{\partial D} \left\{ \frac{\partial v^s_{f_m^{j,p}}}{\partial \nu}(y) v^i_{g_n^p}(y) - \frac{\partial v^i_{g_n^p}}{\partial \nu}(y) v^s_{f_m^{j,p}}(y) \right\} ds(y). \qquad (2.9)
\end{aligned}$$

From (2.7), (2.8) and (2.9), we have

$$\begin{aligned}
& \lim_{n\to\infty} \int_{S^1}\int_{S^1} u^\infty(-\hat{x}, d)\; f_m^{j,p}(d)\; g_n^p(\hat{x})\; ds(\hat{x}) ds(d) \\
= \; & \gamma_2 \int_{\partial D} \left\{ v^s_{f_m^{j,p}} \frac{\partial \Phi(y, z_p)}{\partial \nu(y)} - \frac{\partial v^s_{f_m^{j,p}}}{\partial \nu(y)} \Phi(y, z_p) \right\} ds(y) \\
= \; & \gamma_2 v^s_{f_m^{j,p}}(z_p) \qquad (2.10)
\end{aligned}$$

from the Green formula, where $v^s_{f_m^{j,p}}(\cdot)$ is the scattered wave corresponding to incident wave $v^i_{f_m^{j,p}}(x) = \mathbb{H}[f_m^{j,p}](x)$.

Denote by $E_j^s(x, z_p)$ the scattered wave corresponding to the incident wave $\frac{\partial \Phi(x,z_p)}{\partial x_j}$, which is well defined for every $x \in \mathbb{R}^2 \setminus \overline{\Gamma}$. Then it follows from (2.6), (2.7), the well posedness of the direct scattering problem and the use of interior estimate that

$$E_j^s(x, z_p) = \lim_{m\to\infty} v^s_{f_m^{j,p}}(x), \quad x \in \mathbb{R}^2 \setminus \overline{D}. \tag{2.11}$$

Finally, it follows from (2.10) that

$$\lim_{m\to\infty}\lim_{n\to\infty}\int_{S^1}\int_{S^1} u^\infty(-\hat{x},d)\; f_m^{j,p}(d)\; g_n^p(\hat{x})\; ds(\hat{x})ds(d) = \gamma_2 E_j^s(z_p,z_p). \tag{2.12}$$

We set

$$I_j(z_p) := \frac{1}{\gamma_2}\lim_{m\to\infty}\lim_{n\to\infty}\int_{S^1}\int_{S^1} u^\infty(-\hat{x},d)\; f_m^{j,p}(d)\; g_n^p(\hat{x})\; ds(\hat{x})ds(d). \tag{2.13}$$

Let us mention that the construction of $f_m^{j,p}$ and g_m^p is independent on the unknown crack. Hence $I_j(z_p)$ is computable from our data only.

The reconstruction of the Γ as well as its eventual surface impedance is established by analysing the behavior of (2.12) when z_p approaches a. For this, we need the C^3 smoothness assumption on the regularity of Γ. Precisely, for every point $a \in \Gamma \setminus \{P,Q\}$, there exists a rigid transformation of coordinates under which the image of a is $\mathbf{0}$ and a function $f \in C^3(-r,r)$ such that

$$f(0) = \frac{df}{dx}(0) = 0, \quad D \cap B(\mathbf{0},r) = \{(x,y) \in B(\mathbf{0},r); y > f(x)\} \tag{2.14}$$

in terms of the new coordinates where $B(\mathbf{0},r)$ is the 2-dimensional ball of center $\mathbf{0}$ with radius r. For the points $a \in \Gamma$, we choose the sequence $\{z_p\}_{p\in\mathbb{N}}$ included in $C_{a,\theta}$, where $C_{a,\theta}$ is a cone with center a, angle $\theta \in [0,\frac{\pi}{2})$ and axis $\nu(a)$. The answer to the inverse problem is based on the following theorem.

THEOREM 2.1 *Assume that Γ is of class C^3 and $\sigma_\pm := \sigma_\pm^r + i\sigma_\pm^i$ are complex valued Holder continuous functions with positive lower bounds for their real parts $\sigma_\pm^r$. Then we have the following formulas:*

1. $\mathrm{Re}(I_j(z_p)) =$

$$\begin{cases} \frac{\pm\nu_j(a)}{4\pi|(z_p-a)\cdot\nu(a)|} \pm \nu_j(a)\kappa\sigma_\pm^i(a)\frac{1}{\pi}\ln(|(z_p-a)\cdot\nu(a)|) + O(1), & a \in \Gamma^\pm \setminus \{P,Q\} \\ \textit{(for the impedance boundary conditions)} , & \\ \frac{\mp\nu_j(a)}{2\pi|(z_p-a)\cdot\nu(a)|} + O(1), & a \in \Gamma^\pm \setminus \{P,Q\} \\ \textit{(for the Dirichlet boundary conditions)} . & \end{cases} \tag{2.15}$$

2.

$$\mathrm{Im}(I_j(z_p)) = \begin{cases} \frac{\mp\nu_j(a)}{\pi}\kappa\sigma_\pm^r\ln(|(z_p-a)\cdot\nu(a)|) + O(1), & a \in \Gamma^\pm \setminus \{P,Q\} \\ \textit{(for the impedance boundary conditions)}, & \\ O(1), & a \in \Gamma^\pm \setminus \{P,Q\} \\ \textit{(for the Dirichlet boundary conditions)} . & \end{cases} \tag{2.16}$$

The notation $a \in \Gamma^\pm$ means that the sequence $\{z_p\}$ tends to a from the right $(+)$ (or, the left $(-)$) side of Γ.

2.1 Comments

The formulas (2.15) and (2.16) can be used to provide the following information on the crack:

- A sample of points on the curve and the normals on these points. The points can be given by numerically solving $|\text{Re } I_j(z)| = C$ for constants C large. The normals are obtained as follows
$$\nu(a) = \pm(t\sqrt{\frac{1}{1+t^2}}, \sqrt{\frac{1}{1+t^2}}) \text{ where } t := \lim_{z_p \to a} \frac{\text{Re}I_1(z_p)}{\text{Re}I_2(z_p)}.$$

- Distinguish the parts where we have Dirichlet or Impedance type of boundary conditions. This is a consequence of the following identities for $a \in \Gamma^{\pm} \setminus \{P, Q\}$ and any given $s \in (0, 1)$:
$$\lim_{z_p \to a} \frac{|\text{Im } I_j(z_p)|}{|\ln(|(z_p - a) \cdot \nu(a)|)|^s} = \begin{cases} \infty, & \text{Impedance boundary} \\ 0, & \text{Dirichlet boundary} \end{cases} \tag{2.17}$$

- In addition, in case of impedance type boundary conditions, we can reconstruct the real and the imaginary parts of the surface impedance $\sigma_{\pm}$:
$$\sigma^r_{\pm}(a) = \lim_{z_p \to a} \frac{\pi \sum_{j=1}^{2} \pm\nu_j(a)\text{Im } I_j(z_p)}{\kappa \ln(|(z_p - a) \cdot \nu(a)|)} \tag{2.18}$$
and
$$\sigma^i_{\pm}(a) = -\lim_{z_p \to a} \frac{\pi \sum_{j=1}^{2} \pm\nu_j(a)\text{Re } I_j(z_p) + \frac{1}{4|(z_p-a)\cdot\nu(a)|}}{\kappa \ln(|(z_p - a) \cdot \nu(a)|)}. \tag{2.19}$$

- The formulas (2.18), rewritten as
$$\pm\sigma^r_{\pm}(a) = \lim_{z_p \to a} \frac{\pi \sum_{j=1}^{2} \pm\nu_j(a)\text{Im } I_j(z_p)}{\kappa \ln(|(z_p - a) \cdot \nu(a)|)} \tag{2.20}$$
enables us to know if $a \in \Gamma^+$ or $a \in \Gamma^-$, i.e to distinguish between the two faces of the crack. Indeed, since $\sigma^r(a) > 0$ then if the right hand side of (2.20) is positive then $a \in \Gamma^+$ and if it is negative then $a \in \Gamma^-$.

- We need to point out a misprint in our previous paper [15]. That is in the equality (2.17) (of that paper) we need to change the sign $\pm$ by $\mp$. However, such a misprint does not have serious effects on the other results since later we used the absolute value.

3 Justification of the results

In this section, we give the proof of Theorem 2.1 for the impedance case since for the Dirichlet case the proof is similar and easier. We consider only the case $j = 2$. The case $j = 1$ can be handled in a similar way with the appropriate changes. We start by some preparations. For any given point $a \in \Gamma$, we firstly take the rotation R_a and the translation M_a such that $R_a(\nu(a)) = (0, 1)$, $R_a(a) + M_a = \mathbf{0}$ in the new coordinate system $\tilde{x}$. Under the transform $\tilde{x} := \mathbb{T}(x) := R_a(x) + M_a$, it follows that $\mathbb{T}(\nu(a)) = (0, 1)$, $\mathbb{T}(a) = \mathbf{0}$. The justification of the results is based on the following propositions which give the dominant part of $E_2(x, z)$ for x, z near a.

PROPOSITION 3.1 *1. Impedance boundary condition case. Let $a \in \Gamma^{\pm} \setminus \{P, Q\}$, then there exist $\delta(a) > 0$ and $C > 0$ such that*

$$|E_2^s(z,z) - w^{\pm}_{\sigma(a)}(z,z)| \leq C, \text{ for } z \in B_+(a,\delta(a)) \cap C_{a,\theta}, \tag{3.1}$$

where $B_+(a,\delta(a)) := B(a,\delta(a)) \cap (\mathbb{R}^2 \setminus D)$ and $B(a,\delta(a))$ is the ball of center a and radius $\delta(a)$. 2. Dirichlet boundary conditions. If $a \in \Gamma^+ \setminus \{P, Q\}$, we obtain (3.1) by replacing $w^{\pm}_{\sigma(a)}$ by w_D.

The functions $w^{\pm}_{\sigma(a)}(x,z)$ and w_D are given by $w^{\pm}_{\sigma(a)}(x,z) := \tilde{w}^{\pm}_{\sigma(a)}(\tilde{x},\tilde{z})$ and $w_D(x,z) := \tilde{w}_D(\tilde{x},\tilde{z})$ where $\tilde{w}^{\pm}_{\sigma(a)}(\tilde{x},\tilde{z})$ and $\tilde{w}_D(\tilde{x},\tilde{z})$ satisfy the folowing properties.

PROPOSITION 3.2 *The function $w^{\pm}_{\sigma(a)}(\tilde{x},\tilde{z})$ has the following explicit form*

$$\tilde{w}^{\pm}_{\sigma(a)}(\tilde{x},\tilde{z}) = \frac{-\nu_2(a)}{4\pi}\int_R e^{i(\tilde{x}_1-\tilde{z}_1)\xi_1} e^{-(\tilde{x}_2+\tilde{z}_2)|\xi_1|}\frac{|\xi_1| \pm i\kappa\sigma(a)}{|\xi_1| \mp i\kappa\sigma(a)} d\xi_1$$

$$+i\frac{\nu_1(a)}{4\pi}\int_R e^{i(\tilde{x}_1-\tilde{z}_1)\cdot\xi_1} e^{-(\tilde{x}_2+\tilde{z}_2)|\xi_1|}\frac{\xi_1}{|\xi_1|}\frac{|\xi_1| \pm i\kappa\sigma(a)}{|\xi_1| \mp i\kappa\sigma}(a) d\xi_1, \tag{3.2}$$

while $\tilde{w}_D(\tilde{x},\tilde{z})$ has the form

$$\tilde{w}_D(\tilde{x},\tilde{z}) = +\frac{\nu_2(a)}{4\pi}\int_R e^{i(\tilde{x}_1-\tilde{z}_1)\xi_1} e^{-(\tilde{x}_2+\tilde{z}_2)|\xi_1|} d\xi_1$$

$$-i\frac{\nu_1(a)}{4\pi}\int_R e^{i(\tilde{x}_1-\tilde{z}_1)\xi_1} e^{-(\tilde{x}_2+\tilde{z}_2)|\xi_1|}\frac{\xi_1}{|\xi_1|} d\xi_1. \tag{3.3}$$

In addition,

$$\tilde{w}^{\pm}_{\sigma(a)}(\tilde{x},\tilde{z}) = -\frac{\nu_2(a)}{2\pi(\tilde{x}_2+\tilde{z}_2)} \pm \frac{i\kappa\nu_2(a)\sigma(a)}{\pi}\ln(\tilde{x}_2+\tilde{z}_2) + O(1) \tag{3.4}$$

and

$$\tilde{w}_D(\tilde{x},\tilde{z}) = +\frac{\nu_2(a)}{2\pi(\tilde{x}_2+\tilde{z}_2)} + O(1). \tag{3.5}$$

We consider the following two problems in the coordinate $\tilde{x} = (\tilde{x}_1, \tilde{x}_2)$ for any given $\tilde{z} = (\tilde{z}_1, \tilde{z}_2) \in \mathbb{R}^2_+$. Then $\tilde{w}^{\pm}_{\sigma(a)}(\tilde{x},\tilde{z})$ and $\tilde{w}_D(\tilde{x},\tilde{z})$ are two functions satisfying

$$\begin{cases} \Delta\tilde{w}^{\pm}_{\tilde{\sigma}(a)} = 0, \quad \tilde{x} \in \mathbb{R}^2_+ \\ (\frac{\partial}{\partial\tilde{x}_2}\tilde{w}^{\pm}_{\tilde{\sigma}(a)} \pm i\kappa\tilde{\sigma}(a)\tilde{w}^{\pm}_{\tilde{\sigma}(a)})(\tilde{x},\tilde{z})|_{\tilde{x}_2=0} = -(\frac{\partial}{\partial\tilde{x}_2} \pm i\kappa\tilde{\sigma}(a))\nabla\Gamma(\tilde{x},\tilde{z})\cdot\tau|_{\tilde{x}_2=0}, \end{cases} \tag{3.6}$$

$$\begin{cases} \Delta\tilde{w}_D = 0, \quad \tilde{x} \in \mathbb{R}^2_+, \\ \tilde{w}_D(\tilde{x},\tilde{z})|_{\tilde{x}_2=0} = -\nabla\Gamma(\tilde{x},\tilde{z})\cdot\tau|_{\tilde{x}_2=0} \end{cases} \tag{3.7}$$

respectively, where $\Gamma(\tilde{x},\tilde{z}) = \frac{1}{2\pi}\ln\frac{1}{|\tilde{x}-\tilde{z}|}$ and the subscript D in $\tilde{w}_D(\tilde{x},\tilde{z})$ refers to the Dirichlet boundary condition in (3.7). The vector τ is given by $\tau := R_a(0,1) = (-\nu_1(a), \nu_2(a))$.

This can be proven by expressing

$$\tilde{w}^{\pm}_{\tilde{\sigma}(a)}(\tilde{x},\tilde{z}) = (U_+[\tilde{x}_2]\phi_{\pm})(\tilde{x}_1), \quad \tilde{w}_D(\tilde{x},\tilde{z}) = (U_+[\tilde{x}_2]\phi)(\tilde{x}_1)$$

in R^2_+ with $(U_+[\tilde{x}_2]\phi)(\tilde{x}_1) := \frac{1}{2\pi}\int_R e^{i\tilde{x}_1\xi_1+\tilde{x}_2|\xi_1|}\hat{\phi}(\xi_1,\tilde{z})d\xi_1$ and computing the density functions $\phi_{\pm}$ and ϕ from the boundary value problems (3.6), (3.7), where $\hat{\phi}$ is the 1-dimensional Fourier transform of ϕ, see [17] for explicit computations.

3.1 End of the proof of Theorem 2.1

We recall the notation $\tilde{x} = (\tilde{x}_1, \tilde{x}_2)$, $\tilde{z} = (\tilde{z}_1, \tilde{z}_2)$ and assume that $\tilde{x}_1 = \tilde{z}_1$ and $\tilde{x}_2, \tilde{z}_2 > 0$. We do the computations for $w^+_{\sigma(a)}$. We get the formulas for $w^-_{\sigma(0)}$ by replacing $\nu(a)$ by $-\nu(a)$.

$$w^+_{\sigma(a)}(\tilde{x}, \tilde{z}) = -\frac{\nu_2(a)}{4\pi} \int_R e^{-(\tilde{x}_2+\tilde{z}_2)|\xi_1|} \frac{|\xi_1| + i\kappa\sigma(a)}{|\xi_1| - i\kappa\sigma(a)} d\xi_1$$

$$= -\frac{\nu_2(a)}{4\pi} \int_R e^{-(\tilde{x}_2+\tilde{z}_2)|\xi_1|} d\xi_1 - \frac{\nu_2(a)}{4\pi} \int_R e^{-(\tilde{x}_2+\tilde{z}_2)|\xi_1|} \frac{2i\kappa\sigma(a)}{|\xi_1| - i\kappa\sigma(a)} d\xi_1$$

$$= -\frac{\nu_2(a)}{2\pi(\tilde{x}_2 + \tilde{z}_2)} - \frac{\nu_2(a)}{2\pi} (i\kappa\sigma(a)) \int_R \frac{e^{-(\tilde{x}_2-\tilde{z}_2)|\xi_1|}}{|\xi_1| - i\kappa\sigma(a)} d\xi_1$$

However

$$\int_R \frac{e^{-(\tilde{x}_2+\tilde{z}_2)|\xi_1|}}{|\xi_1| - i\kappa\sigma(a)} d\xi_1 = \int_R \frac{e^{-(\tilde{x}_2+\tilde{z}_2)|\xi_1|}}{|\xi_1| + \kappa\sigma^i(a) - i\kappa\sigma^r(a)} d\xi_1$$

$$= \int_R e^{-(\tilde{x}_2+\tilde{z}_2)|\xi_1|} \frac{|\xi_1| + \kappa\sigma^i(a) + i\kappa\sigma^r(a)}{(|\xi_1| + \kappa\sigma^i(a))^2 + (\kappa\sigma^r(a))^2} d\xi_1$$

$$= \int_R e^{-(\tilde{x}_2+\tilde{z}_2)|\xi_1|} \frac{|\xi_1| + \kappa\sigma^i(a)}{(|\xi_1| + \kappa\sigma^i(a))^2 + (\kappa\sigma^r(a))^2} d\xi_1 + O(1).$$

Now we have

$$\int_R e^{-(\tilde{x}_2+\tilde{z}_2)|\xi_1|} \frac{|\xi_1| + \kappa\sigma^i(a)}{(|\xi_1| + \kappa\sigma^i(a))^2 + (\kappa\sigma^r(a))^2} d\xi_1$$

$$= 2 \int_0^\infty e^{-(\tilde{x}_2+\tilde{z}_2)\xi_1} \frac{\xi_1 + \kappa\sigma^i(a)}{(\xi_1 + \kappa\sigma^i(a))^2 + (\kappa\sigma^r(a))^2} d\xi_1$$

$$= 2 \int_{\kappa\sigma^i(a)}^\infty e^{-(\tilde{x}_2+\tilde{z}_2)(r-\kappa\sigma^i(a))} \frac{r}{r^2 + (\kappa\sigma^r(a))^2} d\xi_1$$

And

$$\int_{\kappa\sigma^i(a)}^\infty e^{-(\tilde{x}_2+\tilde{z}_2)r} \frac{r}{r^2 + (\kappa\sigma^r(a))^2} d\xi_1 = -\ln(\tilde{x}_2 + \tilde{z}_2) e^{-(\tilde{x}_2+\tilde{z}_2)\kappa\sigma^i(a)} + O(1).$$

Hence

$$w^+_{\sigma(a)}(x, z) = \frac{-\nu_2(a)}{2\pi(\tilde{x}_2 + \tilde{z}_2)} + \frac{i\kappa\sigma(a)\nu_2(a)}{\pi} \ln(\tilde{x}_2 + \tilde{z}_2) + O(1).$$

It is clear that for $\tilde{x}_1 = \tilde{z}_1$, we have $\tilde{w}_D(\tilde{x}, \tilde{z}) = 0$.

Coming back to the original coordinates (x, z), we have:

$$w^+(z, z) = -\frac{\nu_2(a)}{4\pi|(z-a)\cdot\nu(a)|} + \frac{i\kappa\sigma(a)\nu_2(a)}{\pi} \ln(|(z-a)\cdot\nu(a)|) + O(1).$$

We end the proof by using Proposition 3.1.

□

3.2 Proof of Proposition 3.1.

We consider the case where $a \in \Gamma^+ \setminus \{P, Q\}$, i.e. the sequence $(z_p)_{p\in\mathbb{N}}$, tending to a, is in the positive side of Γ. The case $a \in \Gamma^-$ can be done by replacing ν and $-\nu$. We show the details of the case $j = 2$.

Let $\tilde{E}^s(x, z_p)$ be the solution of

$$\begin{cases} (\Delta + \kappa^2)\tilde{E}^s(x, z_p) = 0 \text{ in } \mathbb{R}^2 \setminus \overline{D}, \\ (\frac{\partial}{\partial\nu} + i\kappa\sigma(x))\tilde{E}^s(x, z_p) = -(\partial_\nu + i\kappa\sigma(x))\frac{\partial}{\partial x_2}\Phi(x, z_p) \text{ on } \partial D \\ \tilde{E}^s(\cdot, z) \text{ satisfies the Sommerfeld radiation condition.} \end{cases} \tag{3.8}$$

We state $\tilde{H}_\sigma(x, z) := \tilde{E}(x, z) + \frac{\partial}{\partial x_2}\Phi(x, z)$. Hence $\tilde{H}_{\sigma(a)}$ satisfies

$$\begin{cases} (\Delta + \kappa^2)\tilde{H}_\sigma(x, z) = -\nabla\delta(x, z) \cdot (0, 1) \text{ in } \mathbb{R}^2 \setminus \overline{D}, \\ (\frac{\partial}{\partial\nu} + i\kappa\sigma)\tilde{H}_\sigma(x, z) = 0, \text{ on } \partial D \\ \tilde{H}_\sigma(\cdot, z) \text{ satisfies the Sommerfeld radiation condition.} \end{cases} \tag{3.9}$$

Similarly, we set $H_\sigma(x, z) := E(x, z) + \frac{\partial}{\partial x_2}\Phi(x, z)$. Hence $W := H_\sigma - \tilde{H}_\sigma$ satisfies the properties:

$$\begin{cases} (\Delta + \kappa^2)W(x, z) = 0 \text{ in } \mathbb{R}^2 \setminus \overline{D}, \\ (\frac{\partial}{\partial\nu} + i\kappa\sigma)W(x, z) = 0, \text{ on } \Gamma \cap \partial D \end{cases} \tag{3.10}$$

Let B be a ball of center a and radius $r > 0$. The arguments in [5], see also [4], show that $H_{\sigma(a)}$ and $\tilde{H}_{\sigma(a)}$ satisfy the estimates $|H_{\sigma(a)}(x, z)|, |\tilde{H}_{\sigma(a)}(x, z)| \leq \frac{C}{|x-z|}$ and $|\nabla_x H_{\sigma(a)}(x, z)|, |\nabla_x \tilde{H}_{\sigma(a)}(x, z)| \leq \frac{C}{|x-z|^2}$, for $x, z \in B\setminus D$ where C is a positive constant. Hence, in particular, $\|W(\cdot, z)\|_{H^{1/2}(\partial(B\setminus\overline{D})\setminus\Gamma\cap\partial D)}$ is bounded for z near a. With this property and (3.10), we see that $W(\cdot, z)$ satifies the Helmholtz equation in $B \setminus \overline{D}$ and has bounded $H^{-1/2}(\partial D \cap \Gamma)$ and $H^{1/2}(\partial(B \setminus \overline{D}) \setminus \Gamma \cap \partial D)$ norms of the mixed boundary conditions. We choose B small enough so that κ^2 is not an eingenvalue for the mixed problem. From the well posedness of this problem in Sobolev spaces, see [16] or [2], we deduce in particular that $\|W(\cdot, z)\|_{H^1(B\setminus\overline{D})}$ is bounded with respect to z near a.

We choose G to be the Green's function for $(\Delta + \kappa^2)$ in $B \setminus \overline{D}$ with homogeneous Dirichlet condition on $\partial(B \setminus D)$. An integration by parts shows that

$$W(x, z_p) = \int_{\partial(B\setminus\overline{D})} \frac{\partial}{\partial\nu}G(y, x)W(y, z_p)ds(y), \text{ for } x, z_p \text{ in } B \setminus \overline{D}. \tag{3.11}$$

Taking x tending to $\partial(B \setminus \overline{D}$, then using the discontinuity relations of the double layer potential, we get

$$\frac{1}{2}W(x, z_p) = \int_{\partial(B\setminus\overline{D})\setminus(\Gamma\setminus\partial D)} \frac{\partial}{\partial\nu}G(y, x)W(y, z_p)ds(y), \text{ for } x \in \partial(B \setminus \overline{D}), z_p \in B \setminus \overline{D}. \tag{3.12}$$

By a perturbation argument, writting $G = \Gamma_+ + (G - \Gamma_+)$, we prove that $|\frac{\partial}{\partial\nu}G(y, x)|$ is bounded for $y, x \in \partial(B \setminus \overline{D})$. Hence (3.12) implies that necessary $|W(x, z_p)|$ is bounded for $x \in \partial(B \setminus \overline{D})$ and z_p near a. We take a smaller B if necessary to insure that κ^2 is not a Dirichlet eingenvalue of the Laplacian. Then the maxmum principle implies that $|W(x, z_p)|$ is bounded for x and z_p near a.

This means that we can replace in Proposition 3.1 E^s by $\tilde{E}^s$. Hence, we will analyse $\tilde{E}^s$ near the point a.

We introduce $w^s_\sigma(\cdot, z_p)$ as the solution of

$$\begin{cases} (\Delta + \kappa^2) w^s_\sigma(x, z_p) = 0 \text{ in } \mathbb{R}^2 \setminus \overline{D}, \\ (\frac{\partial}{\partial \nu} + i\kappa\sigma(a)) w^s_\sigma(x, z_p) = -(\partial_\nu + i\sigma(a)) \frac{\partial}{\partial x_2} \Phi(\cdot, z_p) \text{ on } \partial D \\ w^s_\sigma(\cdot, z) \text{ satisfies the Sommerfeld radiation condition.} \end{cases} \tag{3.13}$$

We have the following lemma:

LEMMA 3.3 *There exist $\delta(a) > 0$ and $C(R) > 0$ such that*

$$|(\tilde{E}^s - w^s_\sigma)(x, z_p)| \leq C(R),$$

for $z_p \in B(a, \delta(a)) \cap C_{a,\theta}$ and $x \in (\mathbb{R}^2 \setminus D) \cap B(0, R)$, for any $R > 0$ fixed.

Let $w^s_{\sigma(a),\Phi}(\cdot, z)$ be the solution of

$$\begin{cases} (\Delta + \kappa^2) w^s_{\sigma(a),\Phi}(x, z) = 0 \text{ in } \Omega \setminus \overline{D}, \\ (\frac{\partial}{\partial \nu} + i\kappa\sigma(a)) w^s_{\sigma(a),\Phi}(x, z) = -(\frac{\partial}{\partial \nu} + i\kappa\sigma(a)) \frac{\partial}{\partial x_2} \Phi(x, z_p) \text{ on } \partial D \\ w^s_{\sigma(a),\Phi}(\cdot, z) = -\frac{\partial}{\partial x_2} \Phi(x, z_p) \text{ on } \partial\Omega \end{cases} \tag{3.14}$$

and $w^s_{\sigma(a),\Gamma}(\cdot, z)$ be the solution of (3.14) replacing Φ by Γ. Then we have

LEMMA 3.4 *There exists $C > 0$ such that*

$$|(w^s_{\sigma(a)} - w^s_{\sigma(a),\Phi})(x, z)| \leq C, \quad |(w^s_{\sigma(a),\Phi} - w^s_{\sigma(a),\Gamma})(x, z)| \leq C$$

for $z \in \Omega \setminus D$ near D and $x \in \Omega \setminus D$.

We define $w^{s,0}_{\sigma(a)}$ to be the solution of (3.14) replacing Φ by Γ and the Helmholtz equation by the Laplace equation. Then we have

LEMMA 3.5 *There exists $C > 0$ such that $|(w^s_{\sigma(a),\Gamma} - w^{s,0}_{\sigma(a)})(x, z)| \leq C$, for $z \in \Omega \setminus D$ near D and $x \in \Omega \setminus D$.*

Finally, we have

LEMMA 3.6 *There exist $C > 0, \delta(a) > 0$ such that $|(w^{s,0}_{\sigma(a)} - w^+_{\sigma(a)})(z, z)| \leq C$ for $z \in B(a, \delta(a)) \cap C_{a,\theta}$.*

By combining all the lemmas stated above, we end the proof of Proposition 3.1. □

In the next section, we justify the lemmas we used to prove Proposition3.1

3.3 Proof of the auxiliary lemmas

Proof of Lemma 3.3.

We set $R(x, z) := \tilde{E}^s_\sigma(x, z) - w^s_{\sigma(a)}(x, z)$. Then it satisfies

$$\begin{cases} (\Delta + \kappa^2) R(x, z) = 0 \text{ in } \mathbb{R}^2 \setminus \overline{D}, \\ \frac{\partial R(x,z)}{\partial \nu} + i\kappa\sigma(a) R(x, z) = -i\kappa(\sigma(x) - \sigma(a))(\tilde{E}^s(x, z) + \frac{\partial}{\partial x_2} \Phi(x, z)) \quad \text{on} \quad \partial D, \\ R(\cdot, z) \text{ satisfies the Sommerfeld radiation condition.} \end{cases} \tag{3.15}$$

From (3.15), we have the representation:

$$R(x,z) = -\int_{\partial D} i\kappa(\sigma(y)-\sigma(a))G_{\sigma(a)}(y,x)(\tilde{E}^s + \frac{\partial}{\partial x_2}\Phi)(y,z)ds(y), \text{ for } (x,z) \in \mathbb{R}^2 \setminus \overline{D}. \tag{3.16}$$

We know that $(\tilde{E}^s + \frac{\partial}{\partial x_2}\Phi)(y,z) = \tilde{H}_\sigma$ has the estimate $|\tilde{H}_\sigma(y,z)| \leq \frac{C}{|y-z|}$, then from (3.16) and the Holder regularity of $\sigma(x)$, we deduce that

$$|R(x,z)| \leq c\int_{\partial D} |y-a|^\beta \ln(|y-x|)||z-y|^{-1}ds(y).$$

From the inequality $|y-a| \leq c(\theta)|y-z|$ for $y \in \partial D$ and $z \in C_{a,\theta} \cap B(a,\delta(a))$, we have

$$\frac{|y-a|^\beta}{|y-z|} \leq \frac{c(\theta)^\beta C}{|y-z|^{1-\beta}},$$

which implies

$$|R(x,z)| \leq \int_{\partial D} \frac{c(\theta)^\beta C|\ln|y-x||}{|y-z|^{1-\beta}}dy$$

and therefore $|R(x,z)| = O(1)$ for $x \in \mathbb{R}^2 \setminus D$ and $z \in C_{a,\theta} \cap B(0,R)$. □

With similar arguments as for the proof of Lemma 3.3, we prove Lemma 3.4 and Lemma 3.5.

Proof of Lemma 3.6. Since $w^{s,0}_{\sigma(a)}$ satisfies

$$\begin{cases} \Delta w^{s,0}_{\sigma(a)}(x,z) = 0 \text{ in } \Omega \setminus \overline{D}, \\ (\frac{\partial}{\partial\nu} + i\kappa\sigma(a))(w^{s,0}_{\sigma(a)}(\cdot,z)) = -(\frac{\partial}{\partial\nu} + i\kappa\sigma(a))\frac{\partial}{\partial x_2}\Gamma \quad \text{on} \quad \partial D, \\ w^{s,0}_{\sigma(a)}(\cdot,z) = -\frac{\partial}{\partial x_2}(\Gamma) \text{ on } \partial\Omega, \end{cases} \tag{3.17}$$

then it is clear that $G^0_{\sigma(a)} := w^{s,0}_{\sigma(a)}(x,y) + \frac{\partial}{\partial x_2}\Gamma(x,z)$ satisfies

$$\begin{cases} \Delta(G^0_{\sigma(a)})(x,z) = -\frac{\partial}{\partial x_2}\delta(x-z) \text{ in } \Omega \setminus \overline{D}, \\ (\frac{\partial}{\partial\nu} + i\kappa\sigma(a))(G^0_{\sigma(a)})(\cdot,z) = 0 \quad \text{on} \quad \partial D, \\ (G^0_{\sigma(a)})(\cdot,z) = 0 \text{ on } \partial\Omega. \end{cases} \tag{3.18}$$

We can assume that $a = (0,0)$ and $\nu(a) = (0,1)$ by using the rigid transformation of coordinates $T := R_a(\nu(a)) + M_a$ with which (3.18) needs to be replaced by:

$$\begin{cases} \Delta(G^0_{\sigma(a)}oT^T)(x,z) = -\nabla\delta(x-z)\cdot\tau_2 \text{ in } \Omega \setminus \overline{D}, \\ (\frac{\partial}{\partial\nu} + i\kappa\sigma(a))(G^0_{\sigma(a)}oT^T)(\cdot,z) = 0 \quad \text{on} \quad \partial D, \\ (G^0_{\sigma(a)}oT^T)(\cdot,z) = 0 \text{ on } \partial\Omega, \end{cases} \tag{3.19}$$

where $\tau_2 := R_a \begin{bmatrix} 0 \\ 1 \end{bmatrix} = (-\nu_1(a), \nu_2(a))$.

Let $\xi = F(x)$ be the local change of variables

$$\xi_1 = x_1, \quad \xi_2 = x_2 - f(x_1), \tag{3.20}$$

where f is the function defined in the introduction. We have the following properties:

$$\begin{cases} c_1|x-z| \leq |F(x)-F(z)| \leq c_2|x-z|, \\ |F(x)-x| \leq c_3|x|^2, \\ |DF(x)-I| \leq c_4|x| \end{cases} \tag{3.21}$$

for x, z near the point a, where $c_i (i = 1, 2, 3, 4)$ are positive constants, which is due to the hypothesis on the regularity of ∂D.

Let x, z be points near a. From (3.18), we deduce that $\tilde{G}^0_{\sigma(a)}(\xi, \eta) = G^0_{\sigma(a)} o T^T(x, z)$ satisfies:

$$\begin{cases} \nabla_\xi \cdot B(\xi) \nabla_\xi \tilde{G}^0_{\sigma(a)} = -J^T(\xi) \nabla_\xi \delta(\xi - \eta) \cdot \tau_2 \text{ near } F(a), \\ |J^{-T}\nu| B(\xi) \nabla_\xi \tilde{G}^0_{\sigma(a)} \cdot \tilde{\nu} + i\kappa\sigma(a) \tilde{G}^0_{\sigma(a)} = 0 \text{ on } \partial\mathbb{R}^2_+ \text{ near } F(a), \end{cases} \tag{3.22}$$

where $\xi := F(x)$, $\eta := F(z)$, $B := JJ^T$, $J := \frac{\partial \xi}{\partial x}(F^{-1}(\xi))$ and $\tilde{\nu} := (0, 1)$ is the unit normal to $\partial\mathbb{R}^2_+$. We denoted by J^{-T} the adjoint of J^{-1}. We have from (3.21) that

$$|J^T(\xi) - J^T(0)| \leq c|\xi|, \quad |B(\xi) - B(0)| \leq c|\xi|$$

and $J(0) = B(0) = I$.

We set $\Gamma_{\sigma(a)}(x, z) := (w^+_{\sigma(a)} o T^T + \frac{\partial}{\partial x_2} \Gamma o T^T)(x, z) = (w^+_{\sigma(a)} o T^T + \nabla\Gamma \cdot \tau_2)(x, z)$ and write $\tilde{R}(\xi, \eta) := \tilde{G}^0_{\sigma(a)}(\xi, \eta) - \Gamma_{\sigma(a)}(\xi, \eta)$. Then the function $\tilde{R}(\cdot, \eta)$ satisfies

$$\begin{cases} \nabla_\xi \cdot B(\xi) \nabla_\xi \tilde{R} = \nabla_\xi \cdot (I - B) \nabla_\xi \omega^+_{\sigma(a)} o T^T, \\ B(\xi) \nabla_\xi \tilde{R} \cdot \tilde{\nu} + i\kappa\sigma(a) \tilde{R} = (I - B) \nabla_\xi \Gamma_{\sigma(a)} \cdot \tilde{\nu} + i\kappa\sigma(a)(1 - |J^{-T}\nu|^{-1}) \tilde{G}^0_{\sigma(a)}, \end{cases} \tag{3.23}$$

where the first relation holds in $\mathbb{R}^2_+$ near $F(a)$, while the second one is satisfied on $\partial\mathbb{R}^2_+$ near $F(a)$.

Let G be the Neumann Green's function associated to the expression $\nabla_\xi \cdot B(\xi) \nabla_\xi$ on the circle $B(0, r)$ of radius r.

We set $B^+_r := B(0, r) \cap \mathbb{R}^2_+$ and write $\partial B^+_r = S_r \cup S^c_r$ with $S_r := \partial B^+_r \cap \partial F(D)$.

Integrating by parts in (3.23), we obtain:

$$\begin{aligned} \tilde{R}(\xi, \eta) = &\int_{B^+_r} (I - B) \nabla G(z, \xi) \cdot \nabla \omega^+_{\sigma(a)}(z, \eta) dz + \int_{S_r} (I - B) \nabla \omega^+_{\sigma(a)} \cdot \tilde{\nu} G ds(z) \\ &- i\kappa\sigma(a) \int_{S_r} \tilde{R}(z, \eta) G(z, \xi) ds(z) + i\kappa\sigma(a) \int_{S_r} |(1 - J^{-T}\nu)| \tilde{G}_{\sigma(a)}(z, \eta) G(z, \xi) ds(z) \\ &- \int_{S^c_r} (I - B) \nabla \omega_{\sigma(a)} \cdot \tilde{\nu} G ds(z) + \int_{S^c_r} B \nabla \tilde{R} \cdot \tilde{\nu} G ds(z). \end{aligned} \tag{3.24}$$

Similar arguments as in ([17], [15]) show that $\tilde{R}(\xi, \eta) = O(\ln|\xi - \eta|)$. Now, we are going to prove that actually $\tilde{R}(\xi, \eta) = O(1)$. We start by the asymptotic:

$$G(z, \xi) = \Gamma(z, \xi) + \Gamma(z, \xi^*) + O(1) \tag{3.25}$$

$$\frac{\partial}{\partial z_j} G(z, \xi) = \frac{\partial}{\partial z_j} \Gamma(z, \xi) + \frac{\partial}{\partial z_j} \Gamma(z, \xi^*) + O(\ln(z - \xi)) \tag{3.26}$$

which can also be obtained as in [17], where $\xi^* = (\xi_1, -\xi_2)$.

Hence the third and the forth terms of (3.24) are bounded for ξ and η near the point a. Since a is away from S^c_r then the fifth and the sixth terms are also bounded.

The next step is to prove that

$$\int_{B^+_r} (I - B) \nabla G(z, \xi) \cdot \nabla \omega^+_{\sigma(a)}(z, \eta) dz = O(1) \tag{3.27}$$

$$\int_{S_r}(I-B)\nabla\omega^+_{\sigma(a)}(z,\eta)\cdot\tilde{\nu}G(z,\xi)dz=O(1) \tag{3.28}$$

for $\xi=\eta$ with $\eta\in C_{F(a),\theta}$.

For this, we use the explicit form of B, i.e.

$$B(z):=\begin{bmatrix}1 & -f'(z_1)\\ -f'(z_1) & 1+(f')^2(z_1)\end{bmatrix}$$

to write

$$B(z)-B(\eta)=\begin{bmatrix}0 & -f''(\eta_1)(z_1-\eta_1)\\ -f''(\eta_1)(z_1-\eta_1) & 2f'(\eta_1)f''(\eta_1)(z_1-\eta_1)\end{bmatrix}+O(z_1-\eta_1)^2$$

and then

$$B(z)-B(\eta)=\begin{bmatrix}0 & -1\\ -1 & 0\end{bmatrix}f''(\eta_1)(z_1-\eta_1)+O(\eta_1)O(z_1-\eta_1)+O(z_1-\eta_1)^2$$

Hence, we obtain:

$$\int_{B_r^+}(B(\eta)-B(z))\nabla G(z,\xi)\cdot\nabla\Gamma_{\sigma(a)}(z,\eta)dz=$$

$$f''(\eta_1)\int_{B_r^+}(z_1-\eta_1)[\partial_{z_2}G(z,\xi)\partial_{z_1}(\partial_{z_2}\Gamma_{\sigma(a)})(z,\eta)+\partial_{z_1}G(z,\xi)\partial_{z_2}(\partial_{z_2}\Gamma_{\sigma(a)})(z,\eta)]dz+O(1). \tag{3.29}$$

From Proposition 3.2, we get the estimate:

$$\omega^+_{\sigma(a)}(z,\eta)=\nabla\Gamma(z,\eta^*)\cdot\tau_2+O((\ln|z-\eta|)).$$

From this property and (3.25), it is enough to compute the integrals of (3.29) for $\Gamma(z,\xi)$ and $\partial_{z_j}\Gamma(z,\eta^*)$. Hence we have

$$\int_{B_r^+}(B(\eta)-B(z))\nabla G(z,\xi)\cdot\nabla\omega^+_{\sigma(a)}(z,\eta)dz=$$

$$2f''(\eta_1)\int_{B_r^+}(z_1-\eta_1)[\frac{\partial}{\partial_{z_2}}\Gamma(z,\xi)\frac{\partial}{\partial_{z_1}}\nabla\Gamma)(z,\eta^*)\cdot\tau_2+\frac{\partial}{\partial_{z_1}}\Gamma(z,\xi)\frac{\partial}{\partial_{z_2}}(\nabla\Gamma)(z,\eta^*)\cdot\tau_2]dz+O(1)$$

$$=2f''(\eta_1)[-\nu_1(a)\int_{B_r^+}(z_1-\eta_1)[\frac{\partial}{\partial_{z_2}}\Gamma(z,\xi)\frac{\partial}{\partial_{z_1}}(\frac{\partial}{\partial_{z_1}}\Gamma)(z,\eta^*)+\frac{\partial}{\partial_{z_1}}\Gamma(z,\xi)\frac{\partial}{\partial_{z_2}}(\frac{\partial}{\partial_{z_1}}\Gamma)(z,\eta^*)]dz+$$

$$2f''(\eta_1)[\nu_2(a)\int_{B_r^+}(z_1-\eta_1)[\frac{\partial}{\partial_{z_2}}\Gamma(z,\xi)\frac{\partial}{\partial_{z_1}}(\frac{\partial}{\partial_{z_2}}\Gamma)(z,\eta^*)+\frac{\partial}{\partial_{z_1}}\Gamma(z,\xi)\frac{\partial}{\partial_{z_2}}(\frac{\partial}{\partial_{z_2}}\Gamma)(z,\eta^*)]dz+O(1) \tag{3.30}$$

Let us compute the second integral of (3.30). We have:

$$\partial_{z_2}\Gamma(z,\xi)\partial_{z_1}(\partial_{z_2}\Gamma(z,\eta^*))+\partial_{z_1}\Gamma(z,\xi)\partial_{z_2}(\partial_{z_2}\Gamma(z,\eta^*))=$$

$$=-\frac{1}{4\pi^2}[[-2\frac{(z-\xi^*)\cdot(0,1)}{|z-\xi|^2}[(z-\eta^*)\cdot(0,1)\frac{(z-\eta^*)\cdot(1,0)}{|z-\eta^*|^4}]+$$

$$\frac{(z-\xi)\cdot(1,0)}{|z-\xi|^2}[\frac{1}{|z-\eta^*|^2}-2\frac{[(z-\eta^*)\cdot(0,1)]^2}{|z-\eta^*|^4}]] \tag{3.31}$$

which we write as

$$\partial_{z_2}\Gamma_0(z,\xi)\partial_{z_1}(\partial_{z_2}\Gamma_0(z,\eta^*)) + \partial_{z_1}\Gamma_0(z,\xi)\partial_{z_2}(\partial_{z_2}\Gamma_0(z,\eta^*)) = -\frac{1}{4\pi^2}[-I + II - III]$$

where

$$I := 2\frac{(z_2-\xi_2)(z_2+\eta_2)(z_1-\eta_1)}{|z-\xi|^2|z-\eta^*|^4},\ II := \frac{(z_1-\xi_1)}{|z-\xi|^2|z-\eta^*|^2}$$

and

$$III := 2\frac{(z_2+\eta_2)^2(z_1-\xi_1)}{|z-\xi|^2|z-\eta^*|^4}$$

In the following, we estimate the integrals for I, II and III.

Estimating the integral of I

Let us estimate

$$\int_{B_r^+} 2(z_1-\eta_1)\frac{(z_2-\xi_2)(z_2+\eta_2)(z_1-\eta_1)}{|z-\xi|^2|z-\eta^*|^4}dz.$$

Let $r_1 > 0$ and $r_2 > 0$ be such that $(-r_1, r_1)\times(0, r_2) \subset B_r^+$. Since we are interested in $\xi \in S_r$ and $\eta \in C_{F(a),\theta}$, then

$$\int_{B_r^+} 2(z_1-\eta_1)\frac{(z_2-\xi_2)(z_2+\eta_2)(z_1-\eta_1)}{|z-\xi^*|^2|z-\eta^*|^4}dz$$

$$= \int_0^{r_2}\int_{-r_1}^{r_1} 2(z_1-\eta_1)\frac{(z_2-\xi_2)(z_2+\eta_2)(z_1-\eta_1)}{|z-\xi^*|^2|z-\eta^*|^4}dz_1dz_2 + O(1).$$

Hence

$$\int_{B_r^+} (z_1-\eta_1)\frac{(z_2-\xi_2)(z_2+\eta_2)(z_1-\eta_1)}{|z-\xi|^2|z-\eta^*|^4}dz$$

$$= \int_0^{r_2}(z_2-\xi_2)(z_2+\eta_2)[\int_{-r_1}^{r_1}\frac{(z_1-\eta_1)^2}{|z-\xi|^2|z-\eta^*|^4}dz_1]dz_2 + 0(1).$$

However

$$\int_{-r_1}^{r_1}\frac{(z_1-\eta_1)^2}{|z-\xi|^2|z-\eta^*|^4}dz_1 = \int_{-r_1}^{r_1}\frac{(z_1-\eta_1)^2|z-\eta^*|^2}{|z-\xi|^2|z-\eta^*|^6}dz_1$$

$$= \int_{-r_1}^{r_1}\frac{(z_1-\eta_1)^2|z-\xi|^2}{|z-\xi|^2|z-\eta^*|^6}dz_1 + \int_{-r_1}^{r_1}\frac{(z_1-\eta_1)^2[|\xi-\eta^*|^2 + 2(\xi-\eta^*)\cdot(z-\xi)]}{|z-\xi|^2|z-\eta^*|^6}dz_1$$

Remark that

$$|\int_0^{r_2}\int_{-r_1}^{r_1}\frac{(z_2-\xi_2)(z_2+\eta_2)(z_1-\eta_1)^2[|\xi-\eta^*|^2 + 2(\xi-\eta^*)\cdot(z-\xi)]}{|z-\xi|^2|z-\eta^*|^6}dz_1dz_2| \leq$$

$$\int_0^{r_2}\int_{-r_1}^{r_1}\frac{|\xi-\eta*|^2}{|z-\xi||z-\eta^*|^3} + \frac{|\xi-\eta*|}{|z-\eta^*|^3}dz_1dz_2 = O(\frac{|\xi-\eta^*|^2}{\eta_2^2}) + O(\frac{|\xi-\eta^*|}{\eta_2}),$$

which is bounded for $\xi = \eta$.

Now,

$$\int_{-r_1}^{r_1}\frac{(z_1-\eta_1)^2}{|z-\eta^*|^6}dz_1 = \int_{-r_1}^{r_1}\frac{1}{|z-\eta^*|^4}dz_1 - (z_2+\eta_2)^2\int_{-r_1}^{r_1}\frac{1}{|z-\eta^*|^6}dz_1$$

First we have after a change of variables

$$\int_{-r_1}^{r_1}\frac{1}{|z-\eta^*|^4}dz_1 = \int_{\arctan\frac{-r_1-\eta_1}{|z_2+\eta_2|}}^{\arctan\frac{r_1-\eta_1}{|z_2+\eta_2|}}\frac{(\cos\theta)^2}{|z_2+\eta_2|^3}d\theta.$$

Similarly

$$\int_{-r_1}^{r_1} \frac{1}{|z-\eta^*|^6} dz_1 = \int_{\arctan \frac{-r_1-\eta_1}{|z_2+\eta_2|}}^{\arctan \frac{r_1-\eta_1}{|z_2+\eta_2|}} \frac{(\cos\theta)^4}{|z_2+\eta_2|^3} d\theta.$$

We use the formula $(\cos\theta)^4 = (cos\theta)^2 - \frac{1}{8} + \frac{1}{8}cos(4\theta)$. Then we have:

$$\int_{-r_1}^{r_1} \frac{(z_1-\eta_1)^2}{|z-\eta^*|^6} dz_1 = \frac{1}{8|z_2+\eta_2|^3}[[\arctan \frac{r_1-\eta_1}{|z_2+\eta_2|} - \arctan \frac{-r_1-\eta_1}{|z_2+\eta_2|}]-$$

$$\frac{1}{4}[\sin 4(\arctan \frac{r_1-\eta_1}{|z_2+\eta_2|}) - \sin 4(\arctan \frac{-r_1-\eta_1}{|z_2+\eta_2|})]].$$

Then

$$\int_{B_r^+} (z_1-\eta_1) \frac{(z_2+\xi_2)(z_2+\eta_2)(z_1-\eta_1)}{|z-\xi^*|^2|z-\eta^*|^4} dz =$$

$$\int_0^{r_2} \frac{1}{8|z_2+\eta_2|}[\arctan \frac{r_1-\eta_1}{|z_2+\eta_2|} - \arctan \frac{-r_1-\eta_1}{|z_2+\eta_2|}]dz_2 -$$

$$\int_0^{r_2} \frac{1}{32|z_2+\eta_2|}[[\sin 4(\arctan \frac{r_1-\eta_1}{|z_2+\eta_2|}) - \sin 4(\arctan \frac{-r_1-\eta_1}{|z_2+\eta_2|})]]dz_2 + O(1).$$

Hence

$$\int_{B_r^+} (z_1-\eta_1) \frac{(z_2-\xi_2)(z_2+\eta_2)(z_1-\eta_1)}{|z-\xi|^2|z-\eta^*|^4} dz = -\frac{\pi}{8}\ln(\eta_2) + O(1).$$

Similar computations give

$$\int_{B_r^+} \frac{(z_2-\xi_2)(z_2+\eta_2)(z_1-\eta_1)^2}{|z-\xi|^2|z-\eta^*|^4} dz = -\frac{\pi}{8}\ln(\eta_2) + O(1)$$

and

$$\int_{B_r^+} \frac{(z_1-\xi_1)(z_1-\eta_1)}{|z-\xi^*||z-\eta^*|^2} dz = -\frac{\pi}{2}\ln(\eta_2) + O(1).$$

Then, replacing these values in (3.30) by using (3.31), we obtain:

$$\int_{B_r^+} (B(z)-B(\eta))\nabla G(z,\xi)\cdot\nabla w^+_{\sigma(a)}(z,\eta) dz = O(1)$$

for $\xi = \eta$ with $\eta \in C_{F(a),\theta}$. Now,

$$|\int_{B_r^+} (I-B(\eta))\nabla G(z,\xi)\cdot\nabla \omega^+_{\sigma(a)}(z,\eta^*) dz| \le C|\eta| \int_{B_r^+} \frac{1}{|z-\xi|}\frac{1}{|z-\eta^*|^2} = O(1).$$

for ξ and η near 0. We conclude then that

$$|\int_{B_r^+} (I-B(z))\nabla G(z,\xi)\cdot\nabla \omega^+_{\sigma(a)}(z,\eta^*) dz| \le C|\eta| \int_{B_r^+} \frac{1}{|z-\xi|}\frac{1}{|z-\eta^*|^2} = O(1),$$

for $\xi, \eta \in C_{F(a),\theta}$ and $\xi = \eta$.

With similar computations, the second integral of (3.24) is also bounded for $\xi, \eta \in C_{F(a),\theta}$ such that $\xi = \eta$.

Gathering these estimates, we have $\tilde{R}(\xi,\eta) = O(1)$ for $\xi = \eta$, $\eta \in C_{F(a),\theta}$.

We go back to $R(x,z) := G^0_{\sigma(a)}(x,z) - \Gamma_{\sigma(a)}(x,z)$ and we write it as

$$R(x,z) = G^0_{\sigma(a)}(x,z) - \Gamma_{\sigma(a)}(F(x),F(z)) + \Gamma_{\sigma(a)}(F(x),F(z)) - \Gamma_{\sigma(a)}(x,z),$$

and then

$$R(x,z) = \tilde{R}(F(x),F(z)) + [\Gamma_{\sigma(a)}(F(x),F(z)) - \Gamma_{\sigma(a)}(F(x),z)] +$$

$$[\Gamma_{\sigma(a)}(F(x),z) - \Gamma_{\sigma(a)}(x,z)]. \tag{3.32}$$

From previous computations, we have:

$$\tilde{R}(F(z),F(z)) = O(1). \text{ for } z \in C_{a,\theta} \text{ near } a.$$

Arguing as in ([17], pages 835-836), we show that the second and the third terms in (3.32) are bounded.

Finally, going back to the original coordinates, we have:

$$R(z,z) = O(1) \text{ for } z \in B(a,\delta(a)) \cap C_{a,\theta}$$

for some $\delta(a) > 0$. □

4 Numerical tests

In our model problem we take the crack as a half semi-circle with the representation

$$\Gamma = \{x : x = (x_1(s), x_2(s)) = 1.2 \times (\cos s, \sin s), s \in [0,\pi]\}. \tag{4.1}$$

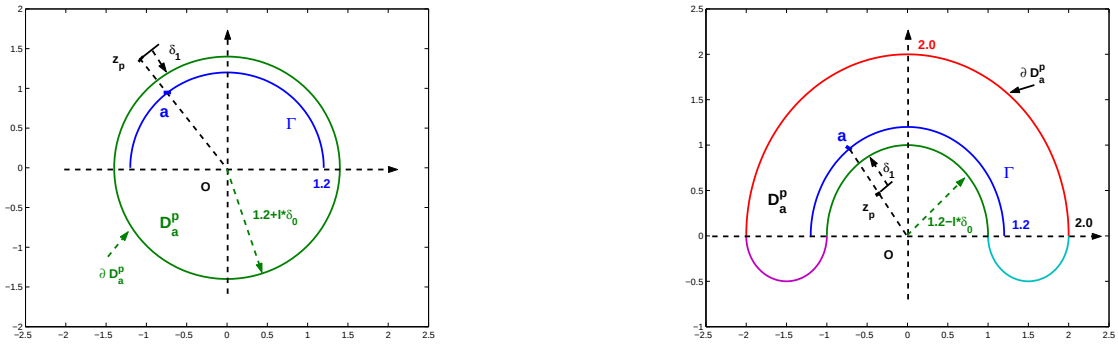

Figure 1: Construction of two D_a^p's. z_p can approach Γ from its convex side using D_a^p in the left-hand side, while D_a^p in the right-hand side is used for z_p approaching Γ from its concave side. When $\delta_1 + l \times \delta_0 \to 0$ with l the approaching step at each direction, $z_p \to a \in \Gamma^{\pm}$ from both sides of Γ along radius direction, respectively.

We check the reconstruction formula for the scattering problem (1.3) which is the most difficult. The other two problems (1.1) and (1.2) can be checked in a similar way. In order to detect the crack Γ as well as its surface impedance $\sigma_{\pm}$, we need to construct some domain D_a^p such that $\Gamma \in D_a^p$ and z_p outside of D_a^p can approach Γ from its two sides. For Γ given by (4.1), we construct two kinds of D_a^p shown in Figure 1. Notice that the parameter $\delta_1 > 0$ represents the singularities

of $\Phi(x,z_p), \partial_{x_i}\Phi(x,z_p)$ for $x \in \partial D_a^p$ near z_p and $l \times \delta_0 > 0$ is the distance between Γ and ∂D_a^p. The sum $\delta_1 + l \times \delta_0$ determines the approximation accuracy $|z_p - a|$ for $a \in \Gamma$. On the other hand, it is easy to see that the domain D_a^p in the right-hand side can also be used for $z_p \to a \in \Gamma$ from the convex part by translating D_a^p along x_2 direction.

We test our inversion method by showing the reconstruction effect for all unknown ingredients in the model: the crack shape, crack type and surface impedance $\sigma_\pm$ in two sides of the crack. We will consider different configurations to show the validity of the method and reveal the physical properties behind the numerical behavior. In fact, we will see that the crack property in the convex side can be distinguished efficiently, while the crack property in the concave side is relatively difficult to be reconstructed numerically. This phenomena comes from the multiple reflection for scattered waves in the concave parts of crack and therefore more energy is absorbed.

Firstly, we use the blowing-up property of the indicator

$$Loc(z_p) := |\mathrm{Re}(I_1(z_p))| + |\mathrm{Re}(I_2(z_p))| \text{ as } z_p \to \Gamma \tag{4.2}$$

to detect the location of crack due to (2.15). That is, when $Loc(z_p)$ is large enough, we consider z_p to be almost on Γ.

Secondly, we use the following equivalent form of the reconstruction formulas (2.18) and (2.19)

$$\lim_{z_p \to a} \frac{\pi \sum_{j=1}^2 \nu_j(a)\mathrm{Im}(I_j(z_p))}{\kappa \ln(|(z_p - a)\cdot \nu(a)|)} = \begin{cases} -\sigma_+^r, & \text{if } z_p \to a \text{ from } \Gamma^+ \\ \sigma_-^r, & \text{if } z_p \to a \text{ from } \Gamma^- \end{cases} \tag{4.3}$$

$$\begin{cases} \lim_{z_p\to a} \frac{\pi \sum_{j=1}^2 \nu_j(a)\mathrm{Re}(I_j(z_p)) - \frac{1}{4|(z_p-a)\cdot\nu(a)|}}{\kappa \ln(|(z_p-a)\cdot\nu(a)|)} = \sigma_+^i, & \text{if } z_p \to a \text{ from } \Gamma^+ \\ \lim_{z_p\to a} \frac{\pi \sum_{j=1}^2 \nu_j(a)\mathrm{Re}(I_j(z_p)) + \frac{1}{4|(z_p-a)\cdot\nu(a)|}}{\kappa \ln(|(z_p-a)\cdot\nu(a)|)} = -\sigma_-^i, & \text{if } z_p \to a \text{ from } \Gamma^- \end{cases} \tag{4.4}$$

for the surface impedance reconstruction as well as for distinguishing Γ^+ from Γ^-. This last property follows from (4.3) since σ^r is assumed to be positive. Hence if the left hand side is positive then we are on the side Γ^- and if not we are on the side Γ^+.

Finally, the crack type is shown by considering the blowing-up property of the function

$$Type(z_p) := \frac{|\mathrm{Im}(I_1(z_p))| + |\mathrm{Im}(I_2(z_p))|}{|\ln|(z_l - a)\cdot\nu(a)||^{1/2}} \text{ as } z_p \to \Gamma \tag{4.5}$$

using the formula (2.17). That is, $Type(z_p)$ should increase up to some value (theoretically ∞) for the impedance crack.

In all the formulas (4.2)-(4.5), z_p are taken along direction t_j to approach the point $a = R_0(\cos t_j, \sin t_j) \in \Gamma$ for all t_j's. In this way, the property of the crack is detected.

In our model problems we take the wave number $\kappa = 1.2$. The far-field pattern data for our inversion are synthesized by solving the direct problem using the combined angular potential and single-layer potential developed in [12].

Example 1 We take the surface impedance as the complex functions of the forms

$$\kappa\sigma_-(x) \equiv 1 + 1.5i, \quad \kappa\sigma_+(x) \equiv 2 + 1.2i \tag{4.6}$$

and use incident plan waves along 64 directions distributed uniformly in $[0, 2\pi]$.

Let $z_p = z(j,l)$ approach to Γ from its convex side. By convex and concave side of crake, we mean the upper side and lower side of Γ given by (4.1), respectively. The crack Γ is detected from 33 directions $t_j = \pi/32 \times j$ with $j = 0, 1, \cdots, 32$. The radius for reconstruction at each direction t_j is determined by the following way. For given blowing-up criterion CB, Let $z(j,l) =$

$(\delta_1 + l \times \delta_0)(\cos t_j, \sin t_j)$ for $l = 16, 15, \cdots, 1$. Here we take $\delta_1 = 0.01, \delta_0 = 0.02$. For any fixed $j = 0, 1, \cdots, 32$, compute the indicator value $Loc(z(j,l))$ defined by (4.2). If this value is larger than CB the first time, we record this step $l(j)$ and the value $C_j := Loc(z(j, l(j)))$. Then we go to the next direction. Using this way, we get the data $\{l(j), C_j\}_{j=0}^{32}$. Compute the average value $C := \sum_{j=0}^{32} C_j/33$. Finally, we compare the value C_j and C and use this perturbation to correct the radius $R_0 + l(j) \times \delta_0$ by linear interpolation as $R_0 + l(j) \times \delta_0 - (C_j - C)/C \times \delta_0$. This is the final radius at direction t_j.

Take the blow-up parameter $CB = 0.8, 1.0, 1.2, 1.3$. The reconstruction results for crack location are given in the left-hand side of Figure 4.2 using the above procedure. Using the technique in [15], we can improve the reconstruction results by combining the reconstructions for different blowing-up criteria together. That is, when the concave closure for the reconstructions with different blowing-up values are taken, the crack will be detected from the convex side with a high accuracy. The only *a-priori* information about the crack is that we know that z_p is in the upper-side of the crack. Notice, in our setting here $\sigma_+^i > 0$. To use our reconstruction formula (2.17) more efficiently, we expect that the reconstruction will be much improved for the case $\sigma_+^i < 0$. However, we need to clarify the physical meaning of this condition. To our knowledge, all the reconstruction problems for surface impedance up to now always consider the case $\sigma_+^i \equiv 0$.

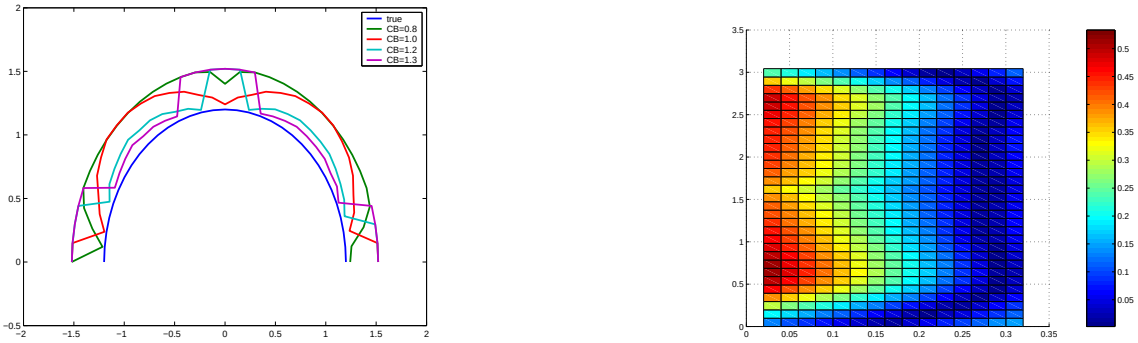

Figure 2: Construction of Γ from the convex side of Γ (left). It can be seen that the tips are not easy to identify with satisfactory accuracy. The crack type detection is shown in the right-hand side. The blowing-up property for the boundary type is obvious, except at the tips.

The crack type detection are checked using (4.5) with the numerical performance given in the right-hand side of Figure 2. The blowing-up property are shown obviously, except at the tips of the crack. Notice, here we use the same singularity to identify the arc shape and the boundary type. It can be shown that the increasing property is quite weak when $z_p \to \Gamma$ along direction $\theta \approx 1.57 \approx \pi/2$. This is reasonable since $\nu_1(a) = 0$ for $a = 1.2(\cos\frac{\pi}{2}, \sin\frac{\pi}{2})$. Therefore $|\mathrm{Im} I_1(z_p)|$ in (4.5) is almost a constant as $z_p \to a$ along the direction $t = \pi/2$ and then the numerator in (4.5) is relatively small, compared with those along other directions.

Now let us recover the boundary impedances $\sigma_\pm$. We need to apply different singularity to detect its real part and imaginary part, respectively.

We take $\delta_0 = 0.1, \delta_1 = 0.1$ for recovering the imaginary part of σ_+. The reconstruction results for $l = 7, 6, 5, 1$ are shown in the left hand side of Figure 3. Noticing $\delta_0 = 0.1$ and the radius of crack is 1.2. For recovering real part of σ_+, we need a strong singularity. Here we take $\delta_0 = 0.01, \delta_1 = 0.003$. The reconstruction for $l = 20, 10, 5, 2, 1$ are given in the right hand side of Figure 3. Notice that the numerical performance is not monotone with respect to l for both real part and imaginary part. Although there are some oscillations for real part of σ_+, the

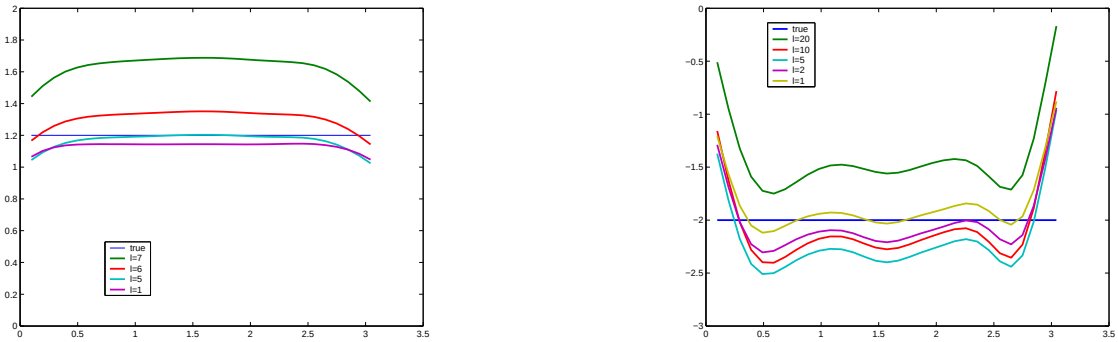

Figure 3: Construction σ_+ from the convex side of Γ: Imaginary part $\kappa\sigma_+^i$ (left) and real part $-\kappa\sigma_+^r$ (right).

reconstruction is satisfactory.

Next we will check the reconstruction of σ_-. Since σ_- is defined in the concave part of Γ, we use D_a^p shown in the right hand side of Figure 1. For recovering its imaginary part, we take $\delta_0 = 0.045, \delta_1 = 0.010$. The results for $l = 6, 4, 2, 1$ are shown in the left-hand side of Figure 4.

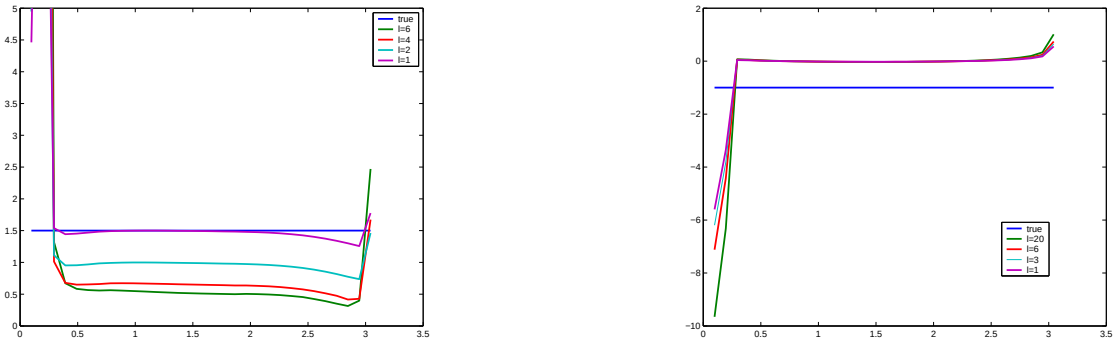

Figure 4: Construction σ_- from the concave side of Γ: Imaginary part $\kappa\sigma_-^i$ (left) and real part $-\kappa\sigma_-^r$ (right). The imaginary part is reconstructed well. For real part, we can only get the distribution behavior, rather than the exact value.

Huge jumps appear at two points $j = 1, 2$. To show thess huge jumps, we list the values near the two tips as follows.

Tab.4.1 Numerical behavior of reconstructing σ_- near the tips.

	$j=1$	$j=2$	$j=3$	$j=30$	$j=31$
$l=6$	10.61619	41.76799	1.320316	0.3975598	2.470905
$l=4$	6.977529	26.65242	1.012647	0.4274354	1.673494
$l=2$	4.947188	17.07493	1.112924	0.7361127	1.462406
$l=1$	4.462630	13.42291	1.539952	1.256604	1.776302

For recovering the real part of σ_-, we take $\delta_0 = 0.002, \delta_1 = 0.001$, a stronger singularity. The results for $l = 10, 6, 3, 1$ are shown in Figure 4 (right). It can be seen that distribution behavior

of σ^r_- is well detected, but the exact value can not be reconstructed well. This phenomena for recovering σ^r_- can also be shown from the other sets of (δ_0, δ_1) with

$$\delta_0 = \delta_1 = 10^{-i}, \quad i = 1, 2, 3, 4.$$

The results as well as its refinement are given in Figure 5.

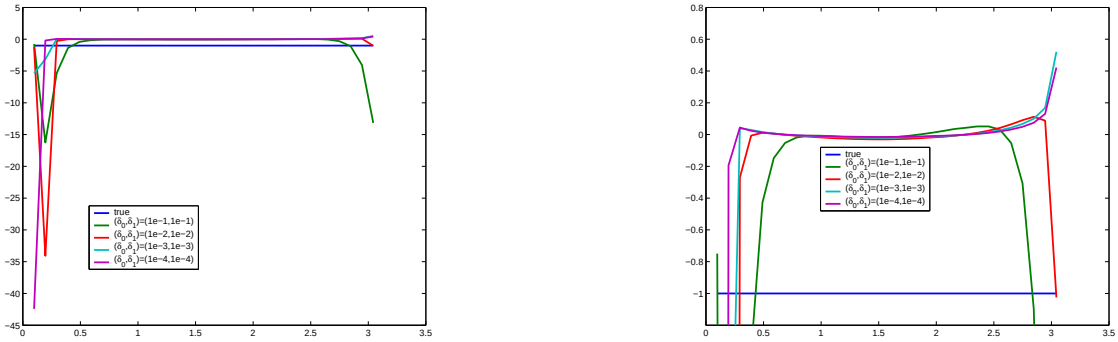

Figure 5: Indicator value for real part of σ^r_- for different sets of (δ_0, δ_1) (left), the right-hand side is its refinement. It can be seen that σ^r_- can not be recovered numerically. However, the distribution behavior of σ^r_- in the interior part of crack is well detected.

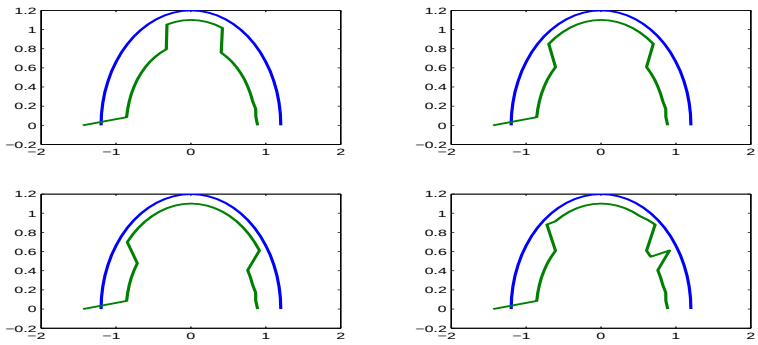

Figure 6: Reconstruction of crack from concave side using the singularity $\delta_0 = 0.02, \delta_1 = 0.001$, where the blowing-up criteria are token as $CB = 0.2, 0.4, 0.9, 1.0$.

The physical background behind this numerical uncertainty for recovering σ^r_- is the multiple reflection of scattered wave in the cavity of the crack Γ in its concave side. Near these concave points, the incident wave will be multi-reflected. For our impedance crack with the energy absorbing coefficient σ^r_- in the concave side, the energy of scattered wave is decreased by each reflection. Therefore the information about the concave side of the crack contained in the far-field pattern is also relatively decreased. We observe also that the multiple reflection of the concave side of the whole crack for a given σ^r_- has the same effects as the other non-concave part of the crack with a higher σ^r_- distribution. Such an energy absorbing phenomena is also studied by engineering, see [8] and the references therein. Due to these reasons, it is understandable that we can not expect too much about the shape reconstruction from the concave side of the crack. Two reconstruction results using formula (4.2) using $z_p \to a \in \Gamma$ from the concave side with $\delta_0 = 0.02, \delta_1 = 0.001$ and

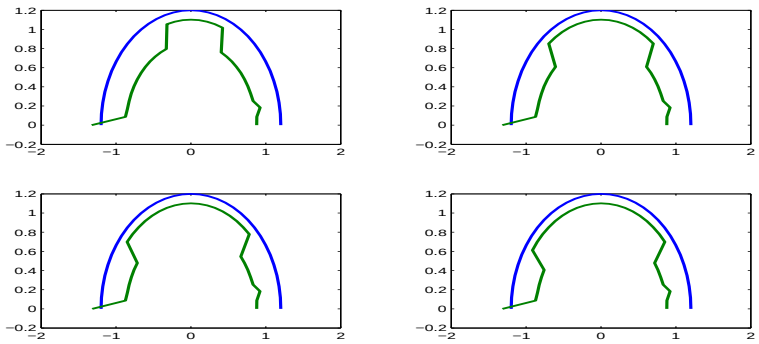

Figure 7: Reconstruction of crack from concave side using $\delta_0 = 0.02, \delta_1 = 0.01$, where the blowing-up criteria are token as $CB = 0.2, 0.4, 0.6, 0.8$.

$\delta_0 = 0.02, \delta_1 = 0.01$ are shown in the following Figure 6 and Figure 7, respectively. In these two figures, we also take $l = 16, \cdots, 1$.

It can be seen that the parts near the two tips can not be identified in the same way as the interior points of the crack. Actually, there si more scattering on these tips than on the interior points on the crack. Notice that the formulas given in section 2 are valid just on the points away from the tips. Also the best approximation accuracy can not be improved. What we can expect is that more part of the crack will be visible using a larger CB but with a finite accuracy. In this configuration, we can not get the blowing-up property of the indicator value numerically since for $\delta_0 = 0.02$ and large l, the distance between z_p and the crack is still large, while the blowing-up property is established theoretically for $l \times \delta_0 + \delta_1 \to 0$.

Our next example is to consider the reconstruction problem where the surface impedance distribution is not constant in the surface, which shows the practical applicability of our reconstruction method.

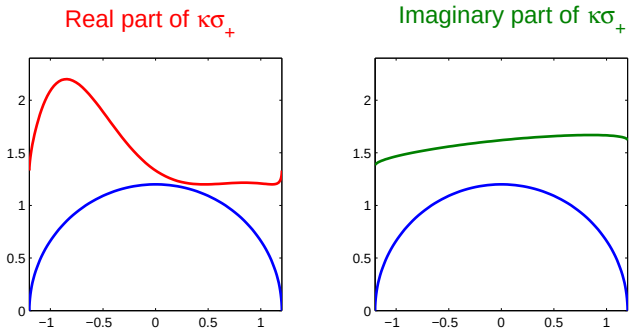

Figure 8: The non-constant distribution of $\kappa\sigma^+$ with respect to variable x_1: real part(left) and imaginary part (right). The half cycle represents the crack.

Example 2. The configuration is taken as follows:

$$\kappa\sigma_+(x) = (\cos^2(x_1 + x_2) + 1.2) + i(\sin\frac{x_1 + x_2}{10} + 1.5), \quad \kappa\sigma_-(x) = (x_1 + 2) + ix_2 \tag{4.7}$$

for $x = (x_1, x_2) \in \Gamma$. The real parts of $\sigma_\pm$ are positive. The distribution of $\kappa\sigma_+$ are shown in

Figure 8. Since we can not expect satisfactory results for the information about Γ_- as explained in Example 1, here we focus on the reconstruction of σ_+ as well as the shape detection from the convex side of crack. We will reveal the effect of the variable surface impedance on the crack shape detection.

We use singularities $\delta_0 = 0.02, 0.01$ to detect the crack shape. The reconstruction result is shown in Figure 9 (left). It can be seen that the reconstruction in domain A is relatively poor. This domain is the part where we have a large value of Re σ_+, compare with Figure 8. The large value of σ_+^r in this domain means a large energy absorbing of the scattered wave. So we can not detect this part using the same singularity as that for the other part. Since σ_+^r is relatively small in the domain B, the the shape detection is well in this part.

As it is done in Example 1, we use the same singularity to detect the boundary type. The numerical behavior of (4.5) in this case is shown in the right-hand side of Figure 9. The vertical variable is the detection direction $t_j = \pi/32 \times j$ for $j = 0, 1, \cdots, 32$. It can be seen that absorbing property of σ_+^r helps us to detect the boundary type obviously. That is, in domain A with large value of σ_+^r, the blowing-up property is obvious. This phenomena is consistent with the detecting formula (2.16).

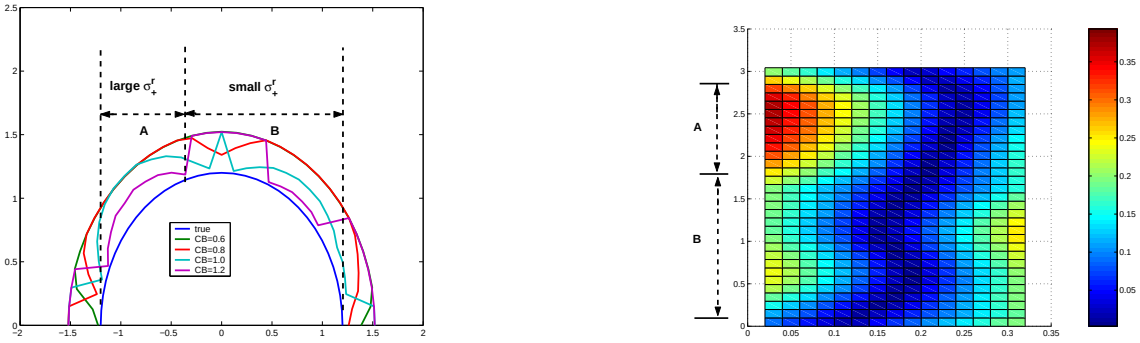

Figure 9: Reconstruction of Γ using $(\delta_0, \delta_1) = (0.02, 0.01)$ with $CB = 0.6, 0.8, 1.0, 1.2$ (left). The crack shape in domain A is not easy to detect due to the large σ_+^r in this part, see the recovery for $CB = 1.0, 1.2$. In the right-hand side, the impedance type is revealed clearly. That is, the larger σ_+^r is, the clearer the impedance type is.

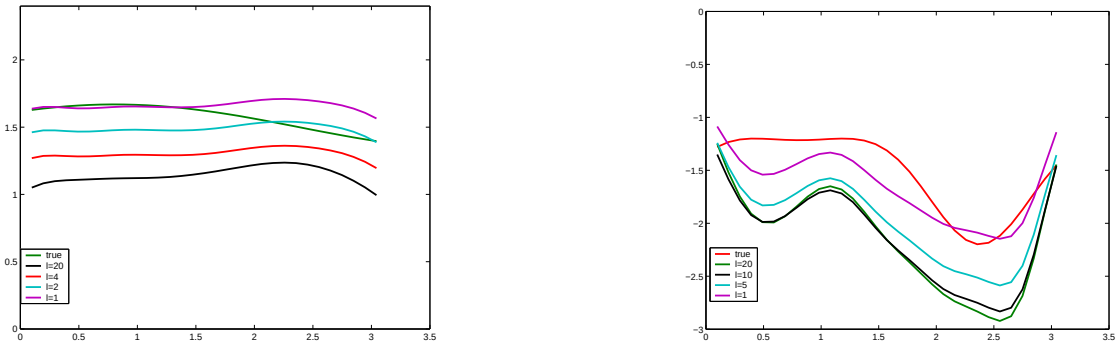

Figure 10: Construction σ_+ from the convex side of Γ: Imaginary part $\kappa\sigma_+^i$ (left) and real part $-\kappa\sigma_+^r$ (right).

Finally, we reconstruct σ_+. To recover the imaginary part of σ_+, we use the singularity $\delta_0 = 0.02, \delta_1 = 0.05$. The results for $l = 20, 4, 2, 1$ are given in the left-hand side of Figure 10. Also we use the singularity $\delta_0 = 0.003, \delta_1 = 0.002$ to detect the real part of σ_+. The results for $l = 20, 10, 5, 1$ are given in the right-hand side of Figure 10.

Example 3: This example is for showing the importance of introducting the artificial coefficient $\mathrm{Im}\sigma_\pm \neq 0$ in the surface impedance. Keep other parameters in Example 1 unchanged, just replace the impedance by

$$\sigma_-(x) \equiv 1 + 2i, \sigma_+(x) \equiv 2 + 5i.$$

Then the arc Γ is reconstructed in Figure 11 (left). The blow-up values are $CB = 1.0, 1.2, 1.5, 1.7$, where we take $z(l) = l \times 0.05$ for $l = 16, 15, \cdots, 1$ to approach $a \in \Gamma$ with $\delta_1 = 0.1$. The reconstruction for crack shape is much better than Example 1 due to the large imaginary part of $\sigma_\pm$. Notice, this picture shows that the points near $(0, 1.2)$ can not be reconstructed well. The reason is that the normal direction is $\nu = (0, 1)$, which means $\nu_1 = 0$. The figure in the right-hand side of Figure 11 shows the boundary detection.

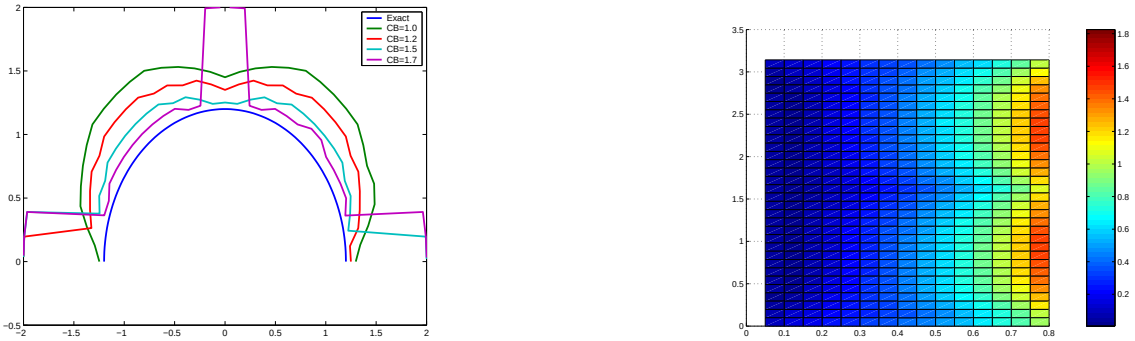

Figure 11: Boundary shape reconstruction and boundary type using the same singularity. It can be seen that the boundary shape is reconstructed well (left). Since $\sigma_\pm$ are large, the crack behaves like a Dirichlet crack., i.e. $Type(z_p) \approx 0$. This phenomena is shown in the right-hand Figure.

Conclusions. In this paper, we consider an inverse scattering problem caused by an open crack Γ. Compared with the inverse scattering problem caused by an impenetrable obstacle with smooth closed boundary, the crack detection problems are much more complicated, due to the joint effects of the tips of crack, the concave side of crack and the inhomogeneous surface impedance distributions. We propose theoretical formulas to detect the property of the crack such as its shape, the boundary type and the surface impedance. The numerical realizations are presented, which show the validity of this method and also some difficulties arising in the detection of concave side of crack. Such difficulties can be explained physically from the multiple reflection of waves in the cavity.

References

[1] K. Bryan and M. S. Vogelius, *A review of selected works on crack identification.* Geometric methods in inverse problems and PDE control, 25–46, IMA Vol. Math. Appl., 137, Springer, New York, 2004.

[2] F. Cakoni, D. Colton, *Qualitative Methods in Inverse scattering Theory*, Interaction of Mechanics and Mathematics, Springer, 2006.

[3] D. Colton, R. Kress, *Inverse Acoustic and Electromagnetic Scattering Theory*, 2nd edition, Berlin-Springer, 1998.

[4] Y. Daido, M. Ikehata, G. Nakamura, Reconstruction of inclusions for the inverse boundary value problem with mixed type boundary condition. Appl. Anal. 83 (2004), no. 2, 109–124.

[5] M. Gruter and K. O. Widman, *The Green function for uniformly elliptic equations*, Manuscripta math, Vol.37, (1982), pp. 303-342.

[6] M. Ikehata *Inverse crack problem and probe method.* Cubo 8 (2006), no. 1, 29–40.

[7] M. Ikehata and G. Nakamura, *Reconstruction formula for identifying cracks.* Essays and papers dedicated to the memory of Clifford Ambrose Truesdell III, Vol. II. J. Elasticity 71 (2003), no. 1-3, 59–72.

[8] K. Goto, T. Ishihara, *High-frequency (Whispering-Gallery Mode)-to-beam conversion on a perfectly conducting concave-convex boundary.* IEEE Transcations on Antennas and Propagation, Vol.50, No.8, (2002), 1109–1119.

[9] P.A. Krutitskii, *Dirichlet's problem for the Helmholtz equation outside cuts in a plane*, Computational Math and Mathematical Physics, Vol.34, No.8/9, (1994), pp. 1073-1090.

[10] P.A. Krutitskii and V.V Kolybasova, *The Helmholtz equation outside cuts on the plane with the Dirichlet condition and a third kind boundary condition on opposite sides of the cuts.* Differential Equations, Vol.42, No.9, (2006), pp. 1247-1261.

[11] P.A. Krutitskii, *The Helmholtz equation in the exterior of slits in a plane with different impedance boundary conditions on opposite sides of the slits*, Quart. Appl. Mathematics, Vol.66, No.4, (2008).

[12] P.A. Krutitskii, J.J. Liu, M. Sini,*Numerical solving the scattering problem of acoustic wave by a crack in 2-dimensional space*, preprint 2008.

[13] R. Kress and K.M. Lee, *Integral equation methods for scattering from an impedance crack*, J. Comput. Appl. Math. 161 (2003), no. 1, 161–177.

[14] W. Littman, G. Stanpacchia and H. F. Weinberger, *Regular points for elliptic equations with discontinuous coefficients*, Ann. Scuola Norm. Sup. Pisa (III), 17, (1963), pp. 43-77.

[15] J.J. Liu, G. Nakamura, M. Sini, *Reconstruction of the shape and surface impedance from acoustic scattering data for an arbitrary cylinder.* SIAM J. Appl. Math. 67 (2007), no. 4, 1124–1146.

[16] W. McLean, *Strongly Elliptic Systems and Boundary Integral Equations.* Cambridge University press, (2000).

[17] G. Nakamura, M. Sini, *Obstacle and boundary determination from scattering data.* SIAM J. Math. Anal, V:39, N: 3 p:819-837.

[18] R. Potthast, *Point Sources and Multipoles in Inverse Scattering Theory*, Research Notes in Mathematics, Vol.427, Chapman-Hall/CRC, Boca Raton, Fl, 2001.

[19] V. A. Solonnikov, *On Green's matrices for elliptic boundary value problems(I)*, Proc. Steklov. Inst. Math,, Vol.110, 1970.

[20] V. A. Solonnikov, *The Green's matrices for elliptic boundary value problems(II)*, Boundary Value Problems of Mathematical Physics, 7, Trudy. Math. Inst. Steklov., Vol.116, (1971), pp. 181-216.